DEC 14, 2011; TO BE PUBLISHED IN *The Astrophysical Journal*.
Preprint typeset using LaTeX style emulateapj v. 5/2/11

A SPECTACULAR OUTFLOW IN AN OBSCURED QUASAR

JENNY E. GREENE
Department of Astrophysical Sciences, Princeton University, Princeton, NJ 08544

NADIA L. ZAKAMSKA
Kavli Institute for Particle Astrophysics and Cosmology, Stanford University, 2575 Sand Hill Road, MS-29, Menlo Park, CA 94025; Kavli Fellow
Department of Physics and Astronomy, Johns Hopkins University, Bloomberg Center, 3400 N. Charles St., Baltimore MD 21218

PAUL S. SMITH
Steward Observatory, University of Arizona, Tucson, AZ 85721
Dec 14, 2011; to be published in The Astrophysical Journal.

ABSTRACT

SDSS J1356+1026 is a pair of interacting galaxies at redshift $z = 0.123$ that hosts a luminous obscured quasar in its northern nucleus. Here we present two long-slit Magellan LDSS-3 spectra that reveal a pair of symmetric ~ 10 kpc-size outflows emerging from this nucleus, with observed expansion velocities of $\sim$250 km s^{-1} in projection. We present a kinematic model of these outflows and argue that the deprojected physical velocities of expansion are likely ~ 1000 km s^{-1} and that the kinetic energy of the expanding shells is likely 10^{44-45} erg s^{-1}, with an absolute minimum of $> 10^{42}$ erg s^{-1}. Although a radio counterpart is detected at 1.4GHz, it is faint enough that the quasar is considered to be radio-quiet by all standard criteria, and there is no evidence of extended emission due to radio lobes, whether aged or continuously powered by an on-going jet. We argue that the on-going star formation is probably insufficient to power the observed energetic outflow and that SDSS J1356+1026 is a good case for radio-quiet quasar feedback. In further support of this hypothesis, polarimetric observations show that the direction of quasar illumination is coincident with the direction of the outflow.

1. INTRODUCTION

The discovery of a tight relationship between the masses of black holes (BHs) in nearby galaxies and the velocity dispersions and masses of their stellar populations (Magorrian et al. 1998; Gebhardt et al. 2000; Ferrarese & Merritt 2000) suggests that the active phase of the supermassive BH evolution has profound effects on the formation of the galaxy. Indeed, there is direct evidence for such 'feedback' by radio-loud active galactic nuclei (AGNs) onto the large-scale gaseous environment of their host galaxies, both at low and at high redshifts (Nesvadba et al. 2008; Fu & Stockton 2009). In these objects, ionized gas is outflowing with velocities above the escape speed from the galaxy, often along the direction of the radio jet. This also appears to be the mode in which AGNs heat up galaxy clusters (McNamara & Nulsen 2007). However, as only a minority ($\sim$10%) of active BHs are radio-loud, this mechanism may not be sufficient to explain the colors and the luminosity function of massive red galaxies (e.g., Springel et al. 2005), and it is as yet unclear if the remaining $\sim$90% of AGNs are affecting the gas, and thus the star formation, in the host galaxies in a similar fashion.

There is strong evidence that star formation driven winds play an important role in galaxy evolution. Their imprint is apparent in the mass-metallicity relation at low redshift (e.g., Tremonti et al. 2004), and they are required in galaxy simulations to reproduce the observations (e.g., Springel et al. 2005; Davé et al. 2008). Most importantly, winds driven by star formation are clearly seen in low-redshift dwarf galaxies (e.g., Martin 1998), in local ultra-luminous infrared galaxies (ULIRGs; e.g., Rupke et al. 2005a), in galaxies at $z \sim 1$ (e.g., Weiner et al. 2009) and high-redshift star-forming galaxies as well (e.g., Shapley et al. 2003). See Veilleux et al. (2005) for a recent review of low redshift observations. What has been much harder to pin down is the role of radio-quiet BH accretion in driving winds (e.g., Tremonti et al. 2007; Alexander et al. 2010; Krug et al. 2010; Coil et al. 2011; Hainline et al. 2011; Rupke & Veilleux 2011).

One class of BHs that may be showing radio-quiet feedback processes in action are broad absorption line quasars, in which high-velocity outflows appear to be driven by the radiation of the quasar itself (e.g., Proga et al. 2000). Because the distance of the outflowing material from the BH and its covering factor are difficult to determine, the kinetic energies of these outflows are unknown in most cases. In some sources, it may be a substantial fraction of the accretion energy (Crenshaw et al. 2003; Moe et al. 2009), and the detailed photo-ionization models place these outflows at a considerable distance (several kpc) from the center of the galaxy (but see also Faucher-Giguere et al. 2011). These observations are promising, but so far have been possible only for a handful of sources. We seek unambiguous evidence for galaxy scale winds.

A handful of strong cases have been made for radiatively driven AGN outflows on galaxy-wide scales at high redshift (e.g., Tremonti et al. 2007; Alexander et al. 2010; Hainline et al. 2011). Locally, new exciting observations of molecular lines, both with ground-based interferometers (Alatalo et al. 2011) and with Herschel (e.g., Fischer et al. 2010) are revealing large molecular outflows that are plausibly AGN-driven. In particular, Sturm et al. (2011) make a strong case that the molecular outflow velocity in local ultra-luminous infrared galaxies (ULIRGs) is strongly correlated with the strength of the active nucleus, such that

more luminous AGNs drive faster outflows (although see also Krug et al. 2010).

Perhaps the best low-redshift case study of large-scale outflows is of Mrk 231. Mrk 231 is the most luminous local ULIRG (Sanders et al. 1988), the nearest broad emission-line AGN, a rare low-ionization broad absorption-line quasar, and contains a radio jet. This galaxy also hosts a massive young starburst that likely dominates the bolometric output of the galaxy (e.g., Lonsdale et al. 2003). The galaxy has been studied in detail at every conceivable wavelength (see, e.g., Feruglio et al. 2010, and references therein). Most relevant to our work are the recent results pointing to a massive molecular (Fischer et al. 2010; Feruglio et al. 2010) and neutral (Rupke & Veilleux 2011) outflow in this galaxy. It is argued strongly in these papers that radiative driving, rather than star formation or jet activity, power the observed outflows. In this paper we try to make a similar case for radiation-pressure driving, except that we focus on a radio-quiet obscured quasar, for which there is little evidence of massive star formation in the optical spectrum. By focusing on obscured, radio-quiet systems, we hope to isolate unambiguously the sources of acceleration in the observed outflows. We also hope to test the hypothesis that AGN feedback occurs most vigorously in the obscured phase (e.g., Sanders et al. 1988; Hopkins et al. 2006).

Since 2007, we have been conducting a study of the morphologies and kinematics of narrow-line regions in obscured radio-quiet quasars (Zakamska et al. 2003; Reyes et al. 2008), in search of tell-tale signs of the interactions between the supermassive BH in its radiative (rather than jet-launching) phase and its large-scale gaseous environment. In our program conducted with the Magellan telescopes (Greene et al. 2009, hereafter Paper I, and Greene et al. 2011, hereafter Paper II), we obtained 15 long-slit spectra of obscured quasars. We find that in the quasar luminosity regime probed by our observations ($L_{[\rm OIII]} \approx 10^{42} - 10^{43}$ erg s^{-1} or inferred $L_{\rm bol} \approx 10^{45} - 10^{46}$ erg s^{-1}), the quasar easily ionizes the galaxy along any direction not obscured by dust. Furthermore, the gas is disturbed on galaxy-wide scales, with both broad emission-line widths and kinematics clearly inconsistent with galaxy rotation. Among these 15 sources, one object, SDSS J135646.10+102609.0 (hereafter SDSS J1356+1026), shows very extended ($\gtrsim$ 50 kpc) ionized line emission which is highly kinematically organized on $\sim$ 20 kpc scales. In this paper, we focus on this source, and build a case for AGN-driven feedback using an analysis of the kinematics and geometry of the ionized gas.

2. OBSERVATIONS AND BASIC OBJECT PROPERTIES

Despite its anonymous telephone number, the enigmatic object SDSS J1356+1026 has already garnered quite a bit of interest in the recent literature. It was targeted for spectroscopy by the Sloan Digital Sky Survey (York et al. 2000) in the Data Release 4 (Adelman-McCarthy et al. 2006). Due to its large [O III]λ5007Å (hereafter [O III]) luminosity and line-ratios indicative of an active nucleus, it was included in the catalog of obscured (type 2) quasars published by Reyes et al. (2008). The kinematic structure of the [O III] line (as seen within the 3″ SDSS spectroscopic fiber) is complex, showing at least two components. As a result, Liu et al. (2010) included SDSS J1356+1026 in a sample of type 2 AGNs with two double-peaked emission lines.

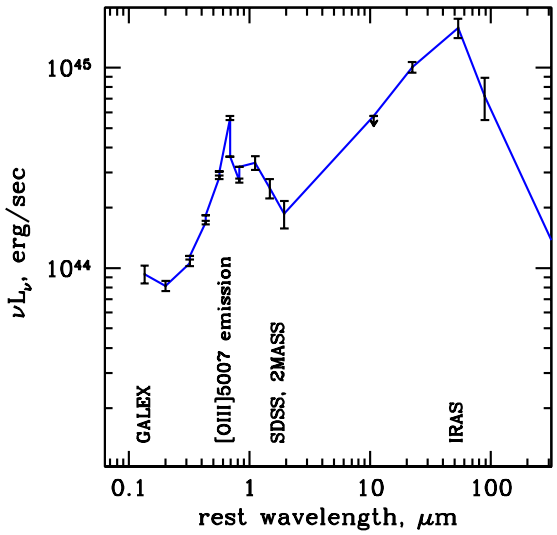

FIG. 1.— The broad-band spectral energy distribution of SDSS J1356+1026. Error bars represent the data presented in Table 1, while the blue line simply connects the points to guide the eye.

Such signatures can be due either to the kinematic structure of the narrow-line region itself or to two quasars, each with its own narrow-line region, with a velocity offset. The galaxy morphology is clearly disturbed, suggesting an ongoing merger (Figure 2 *left*). The presence of two merging galactic nuclei in SDSS J1356+1026 is apparent both in optical (Greene et al. 2009, 2011; Fu et al. 2011a) and in near-infrared (Shen et al. 2011) observations, and strong high-ionization emission lines are associated with both (Paper II and this paper).

The spectroscopic observations of SDSS J1356+1026 were obtained on UT March 18, 2007 using the Low-Dispersion Survey Spectrograph (LDSS3; Allington-Smith et al. 1994) with a $1'' \times 4'$ slit at the Magellan/Clay telescope on Las Campanas. The seeing was $\sim 1''$. We observed with two slit positions for one half hour at each position. Slit position 1 (PA1 hereafter) was oriented north-south, while slit position 2 (PA2 hereafter) was oriented at 45° to the west of PA1 (Figure 2) . We used the VPH-Blue grism in the reddest setting, resulting in wavelength coverage of 4300 – 7050 Å and velocity resolution of $\sigma_{\rm inst} \approx 67$ km s^{-1}. In addition to the primary science targets, at least two flux calibrator stars and a number of velocity template stars were also observed.

Cosmic-ray removal was performed using the spectroscopic version of LACosmic (van Dokkum 2001). Bias subtraction, flat-field correction, wavelength calibration, pattern-noise removal (see Paper I), and rectification were performed using the Carnegie Observatories reduction package COSMOS[1]. The flux calibration correction is determined from the extracted standard star using IDL routines following methods described in Matheson et al. (2008) and then applied in two dimensions. In Paper I we demonstrate that our flux calibration is reliable at the $\sim$ 40% level.

Polarimetric observations were made at the 1.54m Kuiper telescope with SPOL spectropolarimeter (Schmidt et al.

[1] http://obs.carnegiescience.edu/Code/cosmos

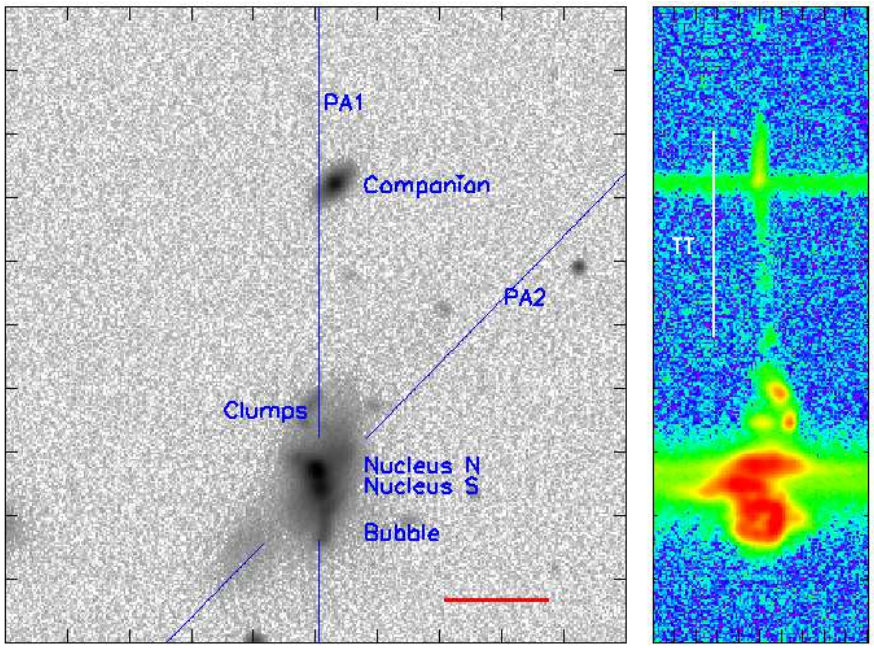

FIG. 2.— *Left*: *r*–band Magellan acquisition image of SDSS J1356+1026 and its immediate environment. Red scale bar indicates 10″ (22 kpc) and blue lines indicate positions of the two spectroscopic slits. N is up and E is to the left. The observation taken with the N-S slit is PA1 and the one with the SE-NW slit is PA2. *Right*: The two-dimensional spectrum centered on [O III]λ5007 taken at the N-S slit position. The vertical scale is the same as that of the image on the left. The full horizontal span is 3842 km s^{-1} centered at 5010Å (rest frame). The "bubble" feature that is the focus of this paper is the round feature to the south of the continuum sources. There is also a tidal feature (TT) connecting the merging galaxies with the companion to the north, with the extent demarcated by the vertical white line.

1992b) on March 29, 2011, with the 3"-wide slit oriented in the E-W direction and an integration time of 32 minutes. The same instrument was again used at the 2.3m Bok telescope on May 27, 2011 with the 3"-wide slit oriented in the N-S direction and an integration time of 40 minutes. In both cases, the polarization measurements span 4000-7550Å with a resolution of $\sim$ 20 Å. The degree of linear polarization (P) is corrected for statistical bias (Wardle & Kronberg 1974) and the position angle of the polarization (θ) was calibrated by observing the interstellar polarization standard stars Hiltner 960 and VI Cyg #12 (Schmidt et al. 1992a). Further details of the general observation and reduction procedures for the spectropolarimetry can be found in Smith et al. (2003).

We have compiled the spectral energy distribution of SDSS J1356+1026 based on publicly available catalogs, from radio to ultra-violet wavelengths (see Table 1; Figure 1). X-ray observations with both *XMM-Newton* and *Chandra* are currently underway.

3. ANALYSIS OF OBSERVATIONS

3.1. *Observed emission*

We first introduce the basic observational components of SDSS J1356+1026 and its immediate environment, as seen in Figure 2. We observe two nuclei, the northern (N) nucleus and the southern (S) nucleus, separated by $\sim$ 2.5 kpc (1.1″) on the sky. We find distinct stellar continuum and ionized gas emission from each nucleus in SDSS J1356+1026. Although the continua are spatially resolved, the southern source is faint enough that we are unable to determine the velocity separation between the nuclei from the stellar spectra. To the north is a companion galaxy located 62 kpc (in projection on the plane of the sky) from the N nucleus. In velocity space, the stellar features of the companion galaxy are blueshifted by $\sim$ 250 km s^{-1} with respect to the stellar features of the N nucleus.

In addition to stellar continua, there is strong, spatially resolved [O III] $\lambda\lambda 4959, 5007$ line emission, as well as Hβ and other high-ionization forbidden lines. We focus here predominantly on the [O III]. A $\sim$ 51 kpc-long [O III] emission line feature (denoted 'TT' for 'tidal tail'; Fig. 2) extends between SDSS J1356+1026 and the northern companion galaxy and somewhat beyond it. No associated stellar continuum is detected for this feature, nor is it seen in the broad-band image. Additional likely tidal features are seen in the broad-band image, such as the low surface brightness feature $\sim$ 10″ (22 kpc) SE of the nuclei. This feature is tentatively detected in [O III] emission in the two-dimensional spectrum (see feature Bv2 in Figure 3).

The focus of this paper is on the well-organized kinematic feature to the South of SDSS J1356+1026, "the bubble" (see Figure 3). The feature appears as a ring in the two-dimensional spectrum, with a spatial extent of $\sim$ 12 kpc and apparent velocity extent of $\sim$ 460 km s^{-1}. The central velocity of the bubble at its base is close to that of the N nucleus, $\sim$ 8 kpc (projected) from its center. Equidistant to the north of the N nucleus, we find three clumps spanning a comparable velocity range. The bubble and the clumps are pure emission-line features, with no stellar continuum detected in the spectra. Emerging at a 45° angle to the bubble are two 'wisps' of emission associated with the same outflow.

We subtract the stellar continuum and co-add the spectrum in velocity space to evaluate the [O III]/Hβ line ratio as a function of position along the slit (Figure 4). The ratio is constant along the slit, with [O III]/Hβ $\sim$ 10, suggesting that the gas is photoionized by an accreting BH. This line ratio is constant for a remarkable number of components, including both the S and N nuclei, bubble, and the northern clumps. We have not corrected these observations for extinction, but note that assuming R_V = 3.1 and the reddening law of Cardelli et al.

TABLE 1
SPECTRAL ENERGY DISTRIBUTION

ν (rest) (Hz)	νL_ν (10^{44} erg s^{-1})	$\sigma(\nu L_\nu)$ (10^{44} erg s^{-1})	source	comment
2.22×10^{15}	0.934	0.097	GALEX far-UV	http://galex.stsci.edu/GalexView/
1.49×10^{15}	0.817	0.049	GALEX near-UV	same
9.39×10^{14}	1.09	0.05	SDSS *u*	http://skyserver.sdss3.org/dr8/en/
6.93×10^{14}	1.77	0.08	SDSS *g*	″
5.36×10^{14}	2.94	0.11	SDSS *r*	″
4.37×10^{14}	4.61	1.01	SDSS *i*	″
3.65×10^{14}	2.97	0.24	SDSS *z*	″
2.70×10^{14}	3.35	0.03	2MASS *J*	http://irsa.ipac.caltech.edu
2.04×10^{14}	2.51	0.03	2MASS *H*	″
1.55×10^{14}	1.87	0.03	2MASS K_S	″
2.81×10^{13}	<5.74		IRAS 12μm	″
1.35×10^{13}	10.1	0.6	IRAS 25μm	″
5.62×10^{12}	15.8	1.7	IRAS 60μm	″
3.37×10^{12}	7.2	1.7	IRAS 100μm	″
1.57×10^{09}	3.40×10^{-4}	0.09×10^{-4}	FIRST and NVSS	Becker et al. (1995); Condon et al. (1998)
4.10×10^{08}	$<3.62\times10^{-4}$		<0.25 Jy (80% completeness limit) in Texas 365 MHz	Douglas et al. (1996)
8.31×10^{07}	$<8.22\times10^{-5}$		<0.28 Jy (2σ) at 74 MHz	Cohen et al. (2007)

NOTE. — **Spectral energy distribution of SDSS J1356+1026 from archival data.** SDSS fluxes are the average of Petrosian and cmodel fluxes. SDSS errors are half of the difference between Petrosian and cmodel fluxes combined in quadrature with the nominal error on the Petrosian fluxes. The large uncertainty in the *i* band is presumably due to the highly disturbed morphology of the object, so that the standard SDSS model fits fail. FIRST and NVSS fluxes are 59.58 mJy and 62.9 mJy, correspondingly. The table entry lists the average of the two, with the uncertainty being half the difference between the two. Although the nominal threshold for the 74 MHz catalog is 5σ = 0.70 Jy, there is no hint of any flux at the source position in the survey stamps, so a 2σ upper limit is adopted. The far-infrared luminosity of SDSS J1356+1026 as estimated using the fitting formula by Sanders & Mirabel (1996) is 2.68×10^{45} erg/sec (the uncertainty is dominated by IRAS flux calibration, $\sim$ 20%). We use an $h = 0.7, \Omega_m = 0.3, \Omega_\Lambda = 0.7$ cosmology.

(1989), there is only an 8% difference in the extinction of Hβ and [O III]. Thus, if we invoke (for instance) higher levels of extinction in the galaxy center, we would still only expect the [O III]/Hβ ratio to decrease by $< 10\%$ in the central region.

As argued in Paper II, the most plausible explanation for the constant line ratios is that both nuclei host obscured quasars with similar luminosities. Another possible scenario is that only one quasar is present and it photo-ionizes the other nucleus; however, we find that the fine-tuning required to satisfy the available observables makes this hypothesis unlikely (Paper II). Future observations (in X-rays with *Chandra* or in the radio with $\sim1''$ resolution) will help distinguish between these two possibilities.

Recently Fu et al. (2011b) presented integral field observations of the $6''\times6''$ field around SDSS J1356+1026 (e.g., largely excluding the bubble itself). It is not obvious from their [O III] map that they see emission line sources associated with both nucleus N and nucleus S. They conclude that SDSS J1356+1026 harbors only a single active black hole in nucleus N, and that the multiple kinematic components are due to large-scale motions of the gas. It is possible that our slit did not intercept the peak emission from nucleus N, thus explaining why the continuum strengths of nucleus S and nucleus N are roughly comparable in our spectrum, even though source N is considerably more luminous (Paper I). We still believe we are seeing a distinct [O III] peak associated with nucleus S, but cannot perform more detailed comparisons at this time.

Taking the spectrum of the bubble alone and subtracting the continuum, we use the velocity profile of the [O III] line to fit all other emission features in the spectrum and thus calculate line ratios without modeling the complex velocity structure of the lines. In particular, we find a ratio of [O III] $\lambda\lambda$4959,5007/[O III] λ4363= 90.5 ± 7.2 and therefore derive an electron temperature $T_e = 13,500\pm500$ K (Osterbrock & Ferland 2006. Furthermore, we detect the [Ar IV]$\lambda\lambda$4711,4730 doublet with a ratio of 1.32 ± 0.37, consistent with its low-density limit of 1.4 (Krueger et al. 1970). Because the critical density for this transition is fairly high, even if we take our measurement as a lower limit on the ratio, it places only a weak limit on the electron density ($n_e \lesssim 850$ cm^{-3}). The ratios of lines of the Balmer series are consistent with no reddening.

The Magellan spectrum does not cover the density diagnostics [O II]$\lambda\lambda$ 3726, 3729 and [S II]$\lambda\lambda$ 6716, 6731, but both of these features are covered by the SDSS spectrum taken in the $3''$circular aperture centered on the nuclei. The components of the [O II] doublet are separated only by 240 km s^{-1} and are far too blended to determine their ratio, given that FWHM$_{[OIII]}$= 652 km s^{-1} in this aperture. The [S II] doublet has an acceptable velocity separation, but the velocity structure of the [O III] emission line does not provide a good fit to this feature, so we cannot determine the line ratio in the same model-independent way as for the Magellan spectrum. We measure the peak ratio of the two components of the doublet to be 1.20, which is likely to be a lower limit on the actual ratio because of blending. Taking [S II] 6716/6731 >1.2 yields $n_e < 250$ cm^{-3}.

The object is strongly linearly polarized, with the polarization fraction reaching 8% at shortest observed wavelengths (Figure 5). These observations are consistent with the hypothesis that SDSS J1356+1026 is powered by a luminous quasar whose emission is largely blocked along the line of sight to the observer, but escapes along some other directions, and then scatters off the interstellar material within the host galaxy (Smith et al. 2003; Zakamska et al. 2005) and reaches the observer. In particular, the emission from the quasar escapes predominantly in the N-S direction in the plane of the sky, as indicated by the $\sim90^\circ$ PA of the plane of polarization. Furthermore, the wavelength dependence of the polar-

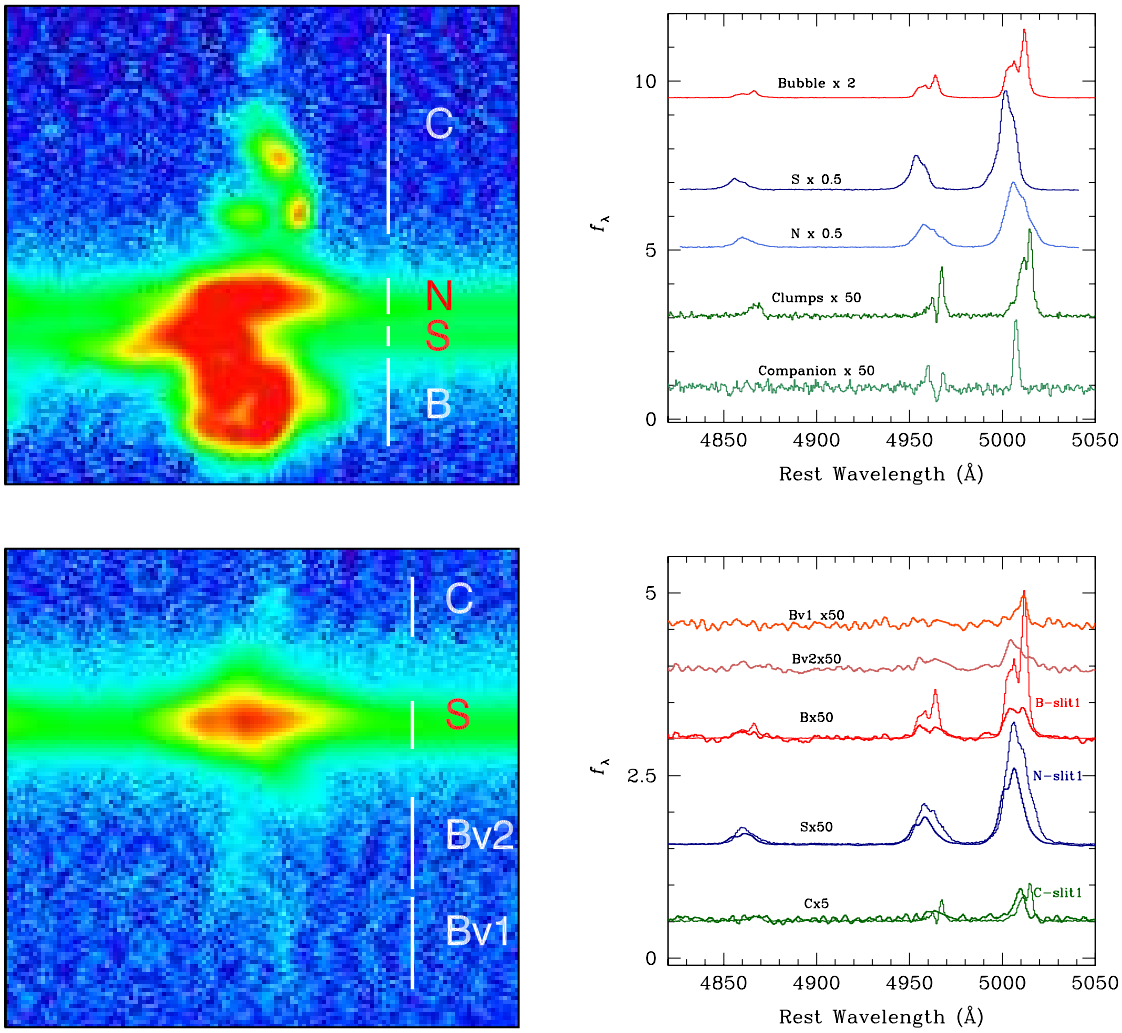

FIG. 3.— Two-dimensional spectra (*left*) and one-dimensional extractions along the labeled regions (*right*) for slit position PA1 (*top*) and PA2 (*bottom*). The two-dimensional spectra are centered on 5007Å and span 80Å (rest-frame) in the spectral direction. Each image is 23″ (50 kpc) in height, although the spectrum along PA2 extends 15 kpc further to the south to highlight Bv1 and Bv2 (the 'wisps'). In the two-dimensional spectra we label features of interest, including, from PA1 (*top left*) – **B**: bubble; **S**: southern nucleus; **N**: northern nucleus; **C**: clumps. We also show the one-dimensional spectrum of the northern Companion seen in Fig. 2 with a 65 kpc projected distance from our program object. We label in PA2 (bottom left) – **Bv1**: wisp feature 1, **Bv2**: wisp feature 2, and **C**: the small amount of flux in the same region as the clumps. The one-dimensional spectra (*right*) are extracted in the windows shown in the two-dimensional image, and the labels correspond, except that the **B** spectrum *bottom right* is the sum of Bv1 and Bv2. The spectra have been multiplied by the factors indicated on the plot for ease of display. In addition, for the PA2 spectra (*bottom right*), we overplot the corresponding features from PA1 to demonstrate the relative velocities between the components. For instance, note that the bubble and the wisps Bv1 and Bv2 have a similar range of velocities. The artifact in the Clump and Companion spectra along PA1 are due to a gap between the two LDSS3 CCDs.

ization fraction can be attributed to the dilution of the scattered quasar light by the unpolarized emission from the extended narrow-line region and starlight from the host galaxy. Indeed, the dilution of the polarized flux by starlight increases to the red, as expected from a red stellar population, and an abrupt minimum in P is seen around [O III] (Figure 5). The generally higher values of P for the N-S slit orientation of the May 27, 2011 observation are likely caused by the fact that the spectral extraction aperture runs along the axis of the presumed scattering cone, thereby including a larger fraction of the scattering regions than the earlier measurement made with the Kuiper Telescope. Other small discrepancies between the two spectropolarimetric observations are likely caused by differing positions of the object within the slit and by the difference in the slit direction, suggesting that polarized structures within the source are partially resolved.

3.2. *Observed Kinematics and Geometry*

We propose that SDSS J1356+1026 is powering a large-scale outflow, which is entraining the warm ionized gas that we see radiating in [O III]. Here we present the observed kinematics along each slit position that we will use to estimate the energetics of the outflow.

Starting with the bubble along the first (NS) slit position PA1, we take two-pixel–wide extractions along the spatial direction starting from nucleus S and working our way to the bottom of the bubble (all within the bubble as demarcated in Figure 3). We use Gaussian fits to identify the primary velocity components at each spatial position. These velocities are plotted in Figure 6, ignoring some weak components. This velocity pattern, increasing symmetrically to a projected velocity of ~ 250 km s^{-1}, is the signature of an expanding sphere of gas with limb brightening.

In addition to the bubble, there are three clumps to the north of nucleus N that we see in slit position PA1. We note that (a) their central velocity is similar to that of the bubble and (b) the

maximum velocity extent across the clumps is comparable to that seen in the bubble (see Figure 3). Therefore, we suggest that these clumps are the northern side of the same outflow. The bubble is systematically blueshifted by ~ 215 km s^{-1} relative to the clumps; therefore, the axis of symmetry of the outflow is likely not quite in the plane of the sky but is tipped so that the bubble is expanding slightly towards us and the clumps are from the component moving slightly away from us (see Figure 6). The northern and southern components of the outflow are discontinuous; we suggest three possible corresponding geometries. One possibility is that we are seeing two unrelated components, but given the similarity of the systemic velocities and the velocity spread we find this unlikely. Another possibility is that our slit did not pass through the center of the outflow, but instead was 1–2″ (2.3-4.6 kpc) offset (see arguments above suggesting that the PA1 slit was not centered on nucleus N). In this case an outflow that forms a figure '8', with the center taken out, could appear as a pair of disconnected features. Yet another possibility (that we favor on the basis of kinematic model presented in the next section) is that the merger provides plentiful gas in the inner several kps of the system, pinching the flow, which finally breaks free of this dense gas on either side, as shown in Figure 5.

The signal-to-noise ratio along PA2 is not very high, and thus we do not measure the velocities as a function of position in this case. The two linear structures to the south of nucleus N, Bv1 and Bv2 (Figure 3) show a clear trend of increasing line-of-sight velocity with projected distance. These wisps represent gas that is escaping at a 45° angle to the gas in the bubble.

3.3. *Kinematic Model*

We see outflowing gas to the north, south, and south-east of the nuclei of SDSS J1356+1026. The emission-line gas is clearly expanding away from the nuclei. Is it being actively driven from the nuclei and accelerating away, or is it decelerating as it slams into the interstellar or intergalactic medium? The linearly expanding structures along PA2 (wisps Bv1 and Bv2) are the tell-tale signs of an accelerating outflow (Veilleux et al. 1994). Both a conical outflow with $v_{3D} \propto r_{3D}$ and a spherical outflow blown from one side with $v_{3D} \propto r_{3D}^2$ will produce $v \propto r$ when projected onto the line of sight (v) and on the plane of the sky (r). The cap of the bubble along the southern-most edge is produced by a shell where the outflow interacts with gas outside the galaxy, either tidal debris or the intergalactic medium. Because of projection effects, the cap is brightest in the plane of the sky, where its line-of-sight velocity is zero, so we do not know whether the shell is still accelerating or whether it has already started to decelerate.

If we assume that there is a single accelerating agent causing all of the outflowing components, then a credible picture of the geometry can be built. Due to interactions with the ambient medium of varying density, the outflow is complicated enough that we cannot uniquely determine its geometry from two slit positions, but we are able to bracket the outflow velocities using a reasonable range of models. Our primary goal is to explain the symmetric velocity structure along the bubble in a way that is also consistent with the clumps to the north and the linearly increasing velocity structures ('wisps') to the south-east along PA2.

We first consider an accelerating ($v_{3D} \propto r_{3D}$) biconical outflow, which is a natural geometry for an obscured quasar and easily explains the wisps.

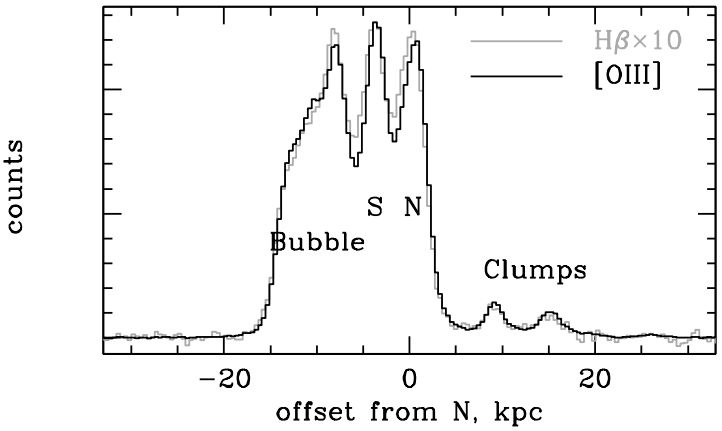

FIG. 4.— The spatial profiles of [O III] and Hβ emission along the N-S slit. The [O III]/Hβ ratio is constant and close to 10.

This model fails to reproduce the concave velocity structure (the southern "cap") observed in the bubble (Figure 6). Another straightforward model is a spherical outflow centered on nucleus N. If only the shell is emitting, it is then difficult to reproduce $v \propto r$ at small radii in the bubble and the wisps. Both the cap and the accelerating features are naturally reproduced in the framework of a bubble blown from its side, not from its center, perhaps due to the high density of matter near the energy injection point (Veilleux et al. 1994). This model is reminiscent of outflows in starburst galaxies, in which propagation in the plane of the galaxy is strongly suppressed and the outflows escape predominantly perpendicular to the plane (Veilleux et al. 2005). Note that if the outflow axis is inclined toward the plane of the sky, then the velocity offset between the clumps and the bubble (relative to the maximum span in the velocity of the bubble) leads to an estimate of the inclination of the axis of $\sim 20°$, which could in principle boost the space velocities relative to those assumed here.

A simple version of this model is shown in Figure 6. We assume that the flow is spherical, with the origin on the side of the sphere and the axis in the plane of the sky, that only the shell is emitting and that $v_{3D} \propto r_{3D}^n$ where $n = 1, 1.5, 2$. Then we project the system onto the sky and the velocities along the line of sight and plot the model curves along with the observations of the bubble in SDSS J1356+1026. We perform a χ^2 fit to the observed position-velocity diagram taking $1 < n < 2.5$. We exclude all data points with velocities greater than ± 400 km s^{-1}, since they are not treated by our model. We further use a minimum velocity error of 20 km s^{-1} (a fraction of a pixel). Models with $1.2 < n < 1.5$ all yield a reduced χ^2 differing from the minimum by less than one. The corresponding range of projected velocities is $250 < v_{3D} < 1000$ km s^{-1}. At the lowest velocity there is no projection effect: the maximum observed velocity is also the maximum space velocity. This is a strict lower limit to the energetics.

We postulate that all of the line emission is part of a quasi-spherical outflow blown by the AGN, that extends from the southern-most edge of the bubble to the clumps in the north (illustrated schematically in Figure 6). However, due to interference from gas and dust in the central pair of galaxies, the outflow cannot escape freely in all directions. Along PA2, the wisps represent gas that has broken free and is in free expansion. In contrast, along the N-S direction (PA1) the outflow

runs into the two galaxies. The ring shape in the PA1 2D spectrum results from gas breaking out of the high density material associated with galaxy S and accelerating away from the merger with $v_{3D} \propto r_{3D}^{1.5}$. In addition, the structure is disconnected from its origin (nucleus N) because of the intervening matter. The clumps in PA1 are the northern counterpart of the same flow, produced closer to nucleus N than the bubble since there is less material to penetrate. In this picture, the similar velocity spread seen along the bubble, clumps and wisps (Fig. 3) are naturally explained as arising from the same outflow. The opening angle of the outflow is no less than the 45° angle between PA1 and PA2, since both slit orientations captured it.

3.4. *Energetics*

With our crude outflow model, and thus deprojected velocities, we can now estimate the energy injection $\dot{E}$ required to power the observed bubble, following Nesvadba et al. (2006). One method is to estimate the kinetic energy in the shell, based on an estimate for the gas mass and the observed velocity, and then divide by the dynamical time to estimate an energy injection rate (e.g., Martin 1998). The other approach is to treat the bubble like a supernova remnant, and estimate the energy needed to expand the bubble into a low-density ambient medium. In both cases we are forced to make assumptions, but with the two methods we can at least bracket the kinetic luminosity of the outflow.

First, we derive a lower limit on the energy in the outflow based on its apparent kinetic energy. The dominant uncertainty here is the mass of gas in the bubble. In principle, with an electron density, we can turn the observed Hβ luminosity ($L_{H\beta} = 7.5 \times 10^{41}$ ergs s^{-1}) into a hydrogen gas mass. As explained in detail in Paper II, we have two methods to estimate gas density in the extended nebulae of obscured quasars. One is the standard diagnostic line ratios, which give density estimates $n_e \lesssim 1000$ cm^{-3}. Unfortunately, this method is biased toward regions of the brightest line emission, and thus regions of the highest density. Furthermore, in clumpy media, density diagnostics often yield values close to the critical density in a wide range of conditions (Paper II). The other method is to use the observations of scattered light at large distances from the nucleus to infer a gas density, but this has only been possible for a couple of objects observed with the *HST* and with particularly well-measured scattered light nebulae (Zakamska et al. 2006). This method gives a mean electron density of $n_e \lesssim 1$ cm^{-3}. Clearly, the two estimates are discrepant, suggesting that gas clumping is significant. Defining the clumping factor as $\kappa = \langle n_e^2 \rangle / \langle n_e \rangle^2$, we can write the mass in gas as:

$$M_g = 1.7 \times 10^9 M_\odot \cdot L_{\mathrm{H}\beta}^{41} \langle n_e \rangle^{-1} \kappa^{-1}. \quad (1)$$

In section 3.1, we used diagnostic line ratios to find that in the nuclear region $n_e < 250$ cm^{-3} and that [O III]/Hβ is constant throughout the nuclei and the bubble. Since at the location of the bubble the ionizing source is 5-10 kpc away, the density must drop with radius by at least a factor of 20–100 to maintain the same ionization parameter (the ratio of the number of ionizing photons to electrons, U). This decrease can plausibly be somewhat offset by a clumping factor of similar magnitude. Therefore, our final mass estimate is $M_g \gtrsim 5 \times 10^7\, M_\odot$. This mass is a lower limit, because it takes into account only the ionized gas that produces emission lines. Any lower density gas at higher temperature filling the bubble would not be included in this estimate.

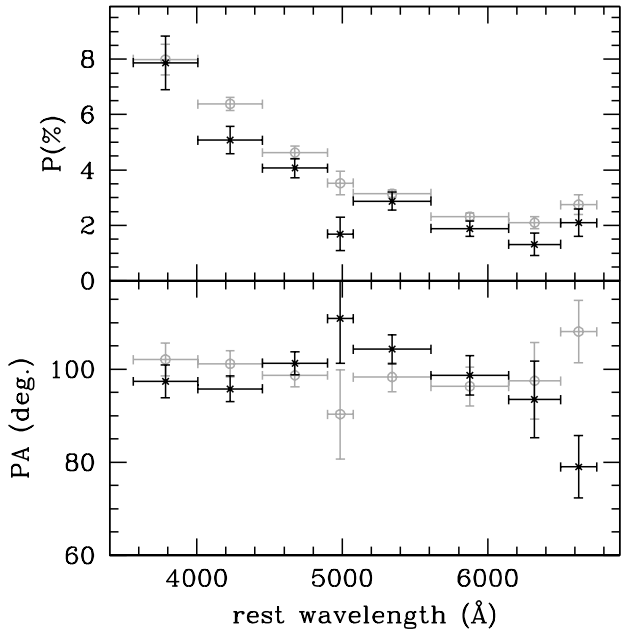

FIG. 5.— *Top*: Polarization fraction. *Bottom*: polarization position angle (degrees E of N) as a function of rest-frame wavelength. Black skeletal points are from the Kuiper telescope observations, with the 3″-wide slit in the E-W direction, and and grey open circles denote binned spectropolarimetry from the Bok telescope, with the 3″-wide slit oriented N-S.

On the other hand, without a measurement of the clumping factor κ, we cannot say for sure what fraction of the observed volume is filled by high-density gas. In the case of the observed bubble in NGC 3079 (e.g., Filippenko & Sargent 1992; Veilleux et al. 1994), the energetics estimates were revised downwards based on high-resolution *HST* imaging of the ionized gas filaments (Cecil et al. 2001). We plan to obtain integral-field observations of SDSS J1356+1026 in the Spring, which will hopefully help settle the outstanding ambiguities.

Based on the extent of the bubble, $R = 12$ kpc, and the maximum deprojected velocity of $v = 250-1000$ km s^{-1}, we find the dynamical time, $t_d \approx R/v \approx 10-40$ Myr. It is interesting to note that this timescale is similar to typical AGN lifetimes (Martini & Weinberg 2001; Martini 2004). With our previous estimate of the mass of the emitting gas, this corresponds to a mass outflow rate of $\dot{M} \sim M_g/t_d > 2-5\, M_\odot$ yr^{-1}. The corresponding kinetic energy is $E_{\mathrm{kin}} \sim M_g v^2/2 > 3-50 \times 10^{55}$ ergs. For a constant energy injection rate over the lifetime of the bubble, we find $\dot{E} > 3-10 \times 10^{41}$ ergs s^{-1}. This is the kinetic energy of the emission line gas alone and, therefore, a strict lower limit on the total energy of the outflow.

The energy injection rate required to expand the bubble into a low-density medium, n_0, in the galaxy halo can be calculated in a manner similar to the Sedov-Taylor solution for supernovae. Following Nesvadba et al. (2006), we assume that the radiative losses are minimal and that energy injection rate is constant rather than a single explosion. We then find

$$\dot{E} \approx 1.5 \times (\Omega/4\pi) 10^{46} R_{10}^2 v_{1000}^3 n_0 \text{ ergs s}^{-1}, \quad (2)$$

where the extent of the bubble R_{10} is in units of 10 kpc, v_{1000} is the expansion velocity in units of 1000 km s^{-1}and $\Omega/4\pi$ is the covering factor of the outflow in steradians. Taking $R_{10} = 1.2$, $n_0 = 0.5$ cm^{-3}, and $v_{1000} = 1$, $\dot{E} \approx (\Omega/4\pi) \times 1.1 \times 10^{46}$ erg s^{-1}.

If we instead adopt the lower limit on velocity (i.e., no deprojection) of $v_{1000} = 0.25$, we find $\dot{E} \approx (\Omega/4\pi) \times 2 \times 10^{44}$ erg s^{-1}.

In addition to the deprojected velocity, the major uncertainty in this value comes from the lack of good measurements of n_0 and Ω. Both slit positions, separated by 45°, captured the signature of the flow and Fu et al. (2011a) find a strong component of [O III] emission to the northeast of N, which is not covered by our observations. We therefore conclude that Ω is not too small. It is much harder to estimate the proper value for n_0. The *HST* observations of Zakamska et al. (2008) alluded to above find clear evidence for electron scattering off of a medium with $n_e \lesssim 1$ cm^{-3}, even at these large projected distances of ~ 10 kpc from the nucleus. We clearly see evidence for denser gas from the observed line emission. Thus, we view our choice of n_0 to be a conservative lower limit.

The kinetic energy injection rate of the outflow is bracketed by the values 10^{42} erg s^{-1} (where we likely underestimated the amount of mass by a large factor) and 10^{46} erg s^{-1} (where we likely overestimated the outflow covering factor and the density of the ambient medium by smaller factors). We will therefore adopt a fiducial range of 10^{44-45} erg s^{-1} for the kinetic energy injection rate in the discussion that follows. It is interesting to note that our upper limit on the kinetic energy injection rate is roughly consistent with our estimate for the radiative bolometric luminosity of $L_{\rm bol} \sim 10^{46}$ ergs s^{-1}.

3.5. *Can the outflow be driven by star formation?*

Can the energy of the outflow be plausibly supplied by any source other than accretion onto the supermassive black hole? Vigorous star formation can lead to large-scale outflows (Veilleux et al. 2005) that are observable both in ionized gas in emission (e.g., Chevalier & Clegg 1985; Heckman et al. 1990) and in neutral gas in absorption (e.g., Rupke et al. 2005b; Martin 2005). In an active merger like SDSS J1356+1026, with plenty of gas available (as evidenced by our emission line observations), it is natural to expect that some on-going star formation is present. While from the high-ionization line ratios (such as the uniformly high [O III]/H$\beta \simeq 10$) it is clear that the photo-ionization of the gas is completely dominated by the quasar, star formation may still be the primary driver of the kinetic outflow. Unfortunately, despite the availability of abundant multi-wavelength data and deep spectra of the host galaxy, the relative contributions of star formation and obscured quasar activity to the bolometric output of SDSS J1356+1026 are very hard to determine. This is a generic difficulty arising due to the fact that most of the flux from the object is coming out at mid- and far-infrared wavelengths, where the emission is due to thermal radiation of dust particles heated by young stars or the quasar in a manner notoriously insensitive to the spectrum of the underlying power source.

The bolometric luminosity of the quasar, as expected from its [O III] luminosity (Liu et al. 2009), is 1.5×10^{46} erg s^{-1}, although such scalings have dispersion of $\gtrsim 0.5$ dex. The bolometric luminosity estimated using the 25 and 60μm IRAS fluxes and quasar bolometric corrections (Richards et al. 2006) ranges between $7.2 \times 10^{45} - 2.4 \times 10^{46}$ erg s^{-1}. The reasonable agreement between these values indicates that most, if not all, of the mid- and far-infrared luminosity from SDSS J1356+1026 (2.7×10^{45} erg s^{-1}) can plausibly be produced by the quasar activity rather than star formation. The high degree of polarization likewise suggests that the AGN is dominant.

If, however, all of the infrared luminosity of this source were powered by star formation, it could just barely power the observed outflow. We use the calculation of the mechanical energy injection rate from a constant rate of star formation by Leitherer & Heckman (1995) and Veilleux et al. (2005). For every solar mass of stars formed, the combination of stellar winds and supernovae can produce at most $L_{\rm mech} \approx 7 \times 10^{41}$ ergs s^{-1} at time $t \approx 10^7$ yr. Thus, to produce a 10^{44-45} erg s^{-1} outflow would require $> 100 - 1000\, M_\odot$ yr^{-1} of star formation and predict a star-formation luminosity of $L_{\rm FIR} = 3 \times 10^{45-46}$ ergs s^{-1}. Thus, star formation is marginally consistent with powering the outflow at the lower limit of the energy range. On the other hand, a starburst of $> 100\, M_\odot$ yr^{-1} is hard to reconcile with our optical spectroscopic and spectropolarimetric observations. We see no evidence in the spectrum for an intermediate age population (i.e., the Balmer absorption lines are consistent with an old stellar population), and the blue continuum that we do see is consistent with scattered light (e.g., Liu et al. 2009). Therefore, we consider power from star formation as unlikely given the currently available data.

3.6. *Can the outflow be jet-driven?*

Radio flux densities at 1.4 GHz can be obtained from the Faint Images of the Radio Sky at Twenty cm survey (FIRST; Becker et al. 1995) and the NRAO VLA Sky Survey (NVSS; Condon et al. 1998). The FIRST detection is unresolved – the nominal deconvolved size of $1.2\times\ 0.6''$ is smaller than half of the beam size of $5.4''$ (Ho & Ulvestad 2001). The FIRST peak flux is 57.90 mJy beam^{-1} and the integrated flux is 59.58 mJy; the ratio of these two measures is consistent with that seen in point sources (Ivezić et al. 2002; Kimball & Ivezić 2008). The high-resolution FIRST observations tend to resolve out the low surface-brightness extended emission, so the comparison with lower-resolution NVSS observations ($45''$ beam) provides yet another measure of extended emission. The NVSS catalog flux is 62.9 mJy, and again the difference between NVSS and FIRST-measured fluxes is consistent with that seen in point sources (Kimball & Ivezić 2008). From these observations, it appears that SDSS J1356+1026 lacks extended radio emission on > 4 kpc ($2''$) scales at the few mJy level.

Using the radio-infrared correlation of star-forming galaxies (Helou et al. 1985) and its convenient normalization presented by Morić et al. (2010), we find that no more than 20% of the observed radio emission can be due to star formation. Thus, most of the radio emission is attributable to one or both quasar nuclei. Nevertheless, the position of the SDSS J1356+1026 in the [O III]-radio diagram (Xu et al. 1999; Zakamska et al. 2004; Lal & Ho 2010) puts it squarely into the radio-quiet regime, 1.5–3 dex below radio-loud sources in Nesvadba et al. (2008) and Fu & Stockton (2009). For direct comparison with Xu et al. (1999), we use a radio spectral index of $\alpha = -0.47$ (defined as $F_\nu \propto \nu^\alpha$, see below) to convert a rest-frame-corrected value of $\log(P_{1.4\rm GHz}, \text{erg s}^{-1}\ \text{Hz}^{-1}) = 31.32$ into $\log(P_{5\rm GHz}, \text{erg s}^{-1}\ \text{Hz}^{-1}) = 31.06$ at $\log(L_{[\rm OIII]}, \text{erg s}^{-1}) = 42.78$ taken from Reyes et al. (2008). Obscured quasars with such radio luminosities have only a $\sim 10\%$ chance to have radio extents > 3 kpc (Lal & Ho 2010), consistent with the lack of any sign of extended emission in SDSS J1356+1026. In principle, we cannot rule out a < 4 kpc-scale jet as the acceler-

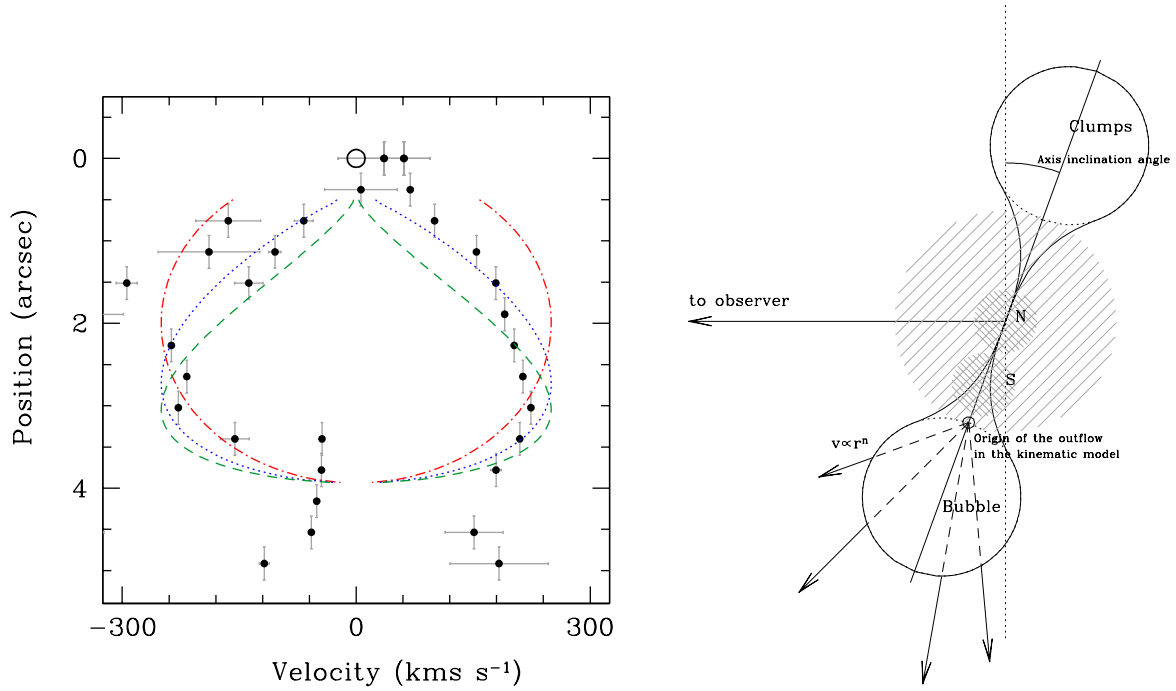

FIG. 6.— We show our simple kinematic model (*left*) and an accompanying cartoon of the outflow region (*right*). *Left*: Position-velocity diagram centered on the the [O III] bubble, as demarcated in Figure 3. Filled black circles indicate velocity peaks measured at intervals of 0.″4. We assume that the accelerating agent is offset from nucleus N by $\sim 2''$, thus the outflow is detached from the continuum source. While the acceleration arises from nucleus N, we show only the outflowing region, starting at the open circle at the origin. Overplotted is a schematic model of a quasi-spherical outflow that is decelerated at its base as it passed through continuum sources N and S. The velocity along the flow increases with radius from source N with a power-law dependence $v \propto r^n$. We plot models with $n = 1$ (*red dash-dot*), $n = 1.5$ (*blue dotted*) and $n = 2$ (*green dashed*). This model yields a maximum outflow velocity of ~ 1000 km s^{-1}. *Right*: A schematic cartoon illustrating our best guess of the system geometry, including the two continuum sources, the Bubble to the south, Clumps to the north, and the slight tilt in the plane of the sky relative to the observer. The circle indicated the origin of our model to the left.

ating agent, as has been proposed for NGC 3079 (Cecil et al. 2001). On the other hand, the outflow we observe is considerably more extended and more energetic than that in NGC 3079, so it is not clear that energy injection on 1 kpc scales can power the observed 20 kpc outflow. Deeper radio interferometry at 1″ resolution would settle the issue.

The source is undetected in the Texas survey at 365 MHz (Douglas et al. 1996) and in the VLA Low-Frequency Survey at 74 MHz (Cohen et al. 2007), with the 74 MHz observation providing a stronger upper limit, so we focus on this observation. This implies a limit on the spectral index $\alpha > -0.47$ (hence the use of this value in the calculation above). Such a flat spectrum effectively excludes a "relic" radio source (Komissarov & Gubanov 1994).

High-resolution, high-sensitivity radio observations would be useful in establishing the presence of two quasars and of any extended radio emission, especially on $5-10''$ scales. Since the separation of the nuclei is $\sim 1''$, observations with VLA would be well-suited for these purposes. The archival radio observations available to us at the moment indicate that the outflow in SDSS J1356+1026 is unlikely to be jet-driven.

4. CONCLUSIONS

SDSS J1356+1026 is an on-going galaxy merger at redshift $z = 0.123$ that contains at least one obscured quasar in its northern nucleus. The bolometric luminosity of the object, estimated at 1.5×10^{46} erg s^{-1}, places it among the more luminous nearby quasars (e.g., Hopkins et al. 2007). We have conducted a study of the kinematics and spatial distribution of the ionized gas in this source. We find a ~ 50 kpc tidal feature close to the systemic velocity of the object that is photoionized by the quasar along an unobscured direction. High optical linear polarization is observed, also indicating that the emission-line regions are powered by the AGN. In addition, we observe a pair of expanding shells, or bubbles, centered on the northern nucleus and expanding into the intergalactic medium. The remarkable scale of the expanding structure (~ 40 kpc in total extent), its high expansion velocities (observed velocity range of 460 km s^{-1}, with physical velocities likely reaching 1000 km s^{-1}), and its large opening angle and luminosity imply that the kinetic energy of the outflow likely exceeds $> 10^{44-45}$ erg s^{-1}.

We find that while star formation may be occurring concurrently with quasar activity in SDSS J1356+1026, it is energetically insufficient to power the observed outflow, likely by an order of magnitude, as further supported by the polarization observations. The merging quasars are radio quiet, and there is no evidence for extended radio emission; therefore, the outflow is unlikely to be powered by a relativistic jet in a manner similar to outflows seen in some radio galaxies. We propose that SDSS J1356+1026 may be an example of on-going feedback from a quasar in its most common radiative phase. Such feedback has been postulated to account for the colors and luminosities of massive galaxies (e.g., Springel et al. 2005), but it has been difficult to assemble direct evidence of interactions between radio-quiet quasars and their large-scale gaseous environments aside from individual cases noted in the introduction. SDSS J1356+1026 provides compelling evidence that accretion energy can drive wide-angle outflows of gas beyond the confines of the host galaxy.

The presence of extended ionized emission by itself is not a

signature of quasar feedback (Stockton & MacKenty 1987). If one could obtain arbitrarily sensitive observations, one would be bound to find small amounts of gas, and if this gas finds itself along an unobscured direction to the quasar it can be photo-ionized out to large distances. For example, Villar-Martín et al. (2010) find a 180 kpc emission-line feature near an SDSS type 2 quasar, but its spatial distribution and kinematics make it clear that the feature is tidal debris illuminated by the quasar. Images of this source taken with the *Hubble Space Telescope* (Zakamska et al. 2006) demonstrate that the scattering regions (and therefore illumination cones) have the same E-W orientation as the 180 kpc tidal tail. We find a very similar feature in SDSS J1356+1026 extending in the N-S direction, which also happens to be the direction of quasar illumination, as indicated by the polarimetric observations. Rather than swept from the galaxy by quasar feedback to 50-100 kpc away, the gas seen in these two cases is most likely tidal debris which happened to be along an unobscured line of sight to the quasar.

Similarly, Liu et al. (2009) find several obscured quasars with companions out to $\gtrsim 30$ kpc away from the quasar showing high equivalent width emission lines with high-ionization line ratios. Again, rather than instances of quasar feedback, these occurrences are probably small companion galaxies which happen to fall within one of the quasar illumination cones.

What sort of signatures specifically implicate quasar feedback? The absence of stellar continuum is a necessary (although not a sufficient) requirement, as it helps rule out illuminated companion galaxies and tidal features. Gas velocities that exceed the escape velocity of the galaxy are a clear sign, but since the outflows from type 2 quasars are directed in the plane of the sky, the chances of observing such high velocities in these objects are low. The presence of a kinematically organized and symmetric structure, such as that seen in SDSS J1356+1026, is a very compelling clue, as it completely rules out an instance of a gas inflow illuminated by the quasar (while the nature of radial velocity observations technically makes inflow and outflow scenarios degenerate, it is hard to imagine the gas conspiring to accrete in such symmetric manner). The high linear-polarization fraction of $P = 8\%$ provides unambiguous evidence that there is a luminous obscured quasar in SDSS J1356+1026 and severely limits the fraction of the bolometric luminosity of this source that may be due to star formation. Furthermore, through the measurement of the polarization position angle, polarimetric observations indicate that the outflow direction (N-S) is well aligned with the predominant direction of quasar illumination. Clearly a narrow-band image or integral-field spectroscopy would provide a more complete picture of the energetics.

We did not find similarly well-organized kinematics in the rest of the Magellan sample (Greene et al. 2011), but the large velocity widths and the lack of rotation seen even in prominent disk galaxies observed along their semi-major axes make quasar feedback the likely explanation in those cases as well. Our work to study three-dimensional outflows in luminous obscured quasars is ongoing with integral-field spectroscopy, which we hope will provide better statistics on the population as a whole (Zakamska, N. L. et al. in preparation).

The referee made valuable comments that significantly improved this manuscript. We gratefully acknowledge useful conversations with Daniel Proga. We also thank L. C. Ho and A. J. Barth for invaluable assistance in the earlier stages of this project. P.S.S. acknowledges support from NASA/Fermi Guest Investigator Program grant NNX09AU10G.

REFERENCES

Adelman-McCarthy, J. K., et al. 2006, ApJS, 162, 38
Alatalo, K., et al. 2011, ApJ, 735, 88
Alexander, D. M., Swinbank, A. M., Smail, I., McDermid, R., & Nesvadba, N. P. H. 2010, MNRAS, 402, 2211
Allington-Smith, J., et al. 1994, PASP, 106, 983
Becker, R. H., White, R. L., & Helfand, D. J. 1995, ApJ, 450, 559
Cardelli, J. A., Clayton, G. C., & Mathis, J. S. 1989, ApJ, 345, 245
Cecil, G., Bland-Hawthorn, J., Veilleux, S., & Filippenko, A. V. 2001, ApJ, 555, 338
Chevalier, R. A., & Clegg, A. W. 1985, Nature, 317, 44
Cohen, A. S., Lane, W. M., Cotton, W. D., Kassim, N. E., Lazio, T. J. W., Perley, R. A., Condon, J. J., & Erickson, W. C. 2007, AJ, 134, 1245
Coil, A. L., Weiner, B. J., Holz, D. E., Cooper, M. C., Yan, R., & Aird, J. 2011, ApJ, accepted (arXiv:1104.0681)
Condon, J. J., Cotton, W. D., Greisen, E. W., Yin, Q. F., Perley, R. A., Taylor, G. B., & Broderick, J. J. 1998, AJ, 115, 1693
Crenshaw, D. M., Kraemer, S. B., & George, I. M. 2003, ARA&A, 41, 117
Davé, R., Oppenheimer, B. D., & Sivanandam, S. 2008, MNRAS, 391, 110
Douglas, J. N., Bash, F. N., Bozyan, F. A., Torrence, G. W., & Wolfe, C. 1996, AJ, 111, 1945
Faucher-Giguere, C. ., Quataert, E., & Murray, N. 2011, MNRAS, submitted (arXiv:1108.0413)
Ferrarese, L., & Merritt, D. 2000, ApJ, 539, L9
Feruglio, C., Maiolino, R., Piconcelli, E., Menci, N., Aussel, H., Lamastra, A., & Fiore, F. 2010, A&A, 518, L155
Filippenko, A. V., & Sargent, W. L. W. 1992, AJ, 103, 28
Fischer, T. C., Crenshaw, D. M., Kraemer, S. B., Schmitt, H. R., & Trippe, M. L. 2010, AJ, 140, 577
Fu, H., Myers, A. D., Djorgovski, S. G., & Yan, L. 2011a, ApJ, 733, 103
Fu, H., & Stockton, A. 2009, ApJ, 690, 953
Fu, H., Yan, L., Myers, A. D., Stockton, A., Djorgovski, S. G., Aldering, G., & Rich, J. A. 2011b, ArXiv e-prints
Gebhardt, K., et al. 2000, ApJ, 539, L13
Greene, J. E., Zakamska, N. L., Ho, L. C., & Barth, A. J. 2011, ApJ, 732, 9
Greene, J. E., Zakamska, N. L., Liu, X., Barth, A. J., & Ho, L. C. 2009, ApJ, 702, 441
Hainline, K. N., Shapley, A. E., Greene, J. E., & Steidel, C. C. 2011, ApJ, 733, 31
Heckman, T. M., Armus, L., & Miley, G. K. 1990, ApJS, 74, 833
Helou, G., Soifer, B. T., & Rowan-Robinson, M. 1985, ApJ, 298, L7
Ho, L. C., & Ulvestad, J. S. 2001, ApJS, 133, 77
Hopkins, P. F., Hernquist, L., Cox, T. J., Di Matteo, T., Robertson, B., & Springel, V. 2006, ApJS, 163, 1
Hopkins, P. F., Richards, G. T., & Hernquist, L. 2007, ApJ, 654, 731
Ivezić, Ž., et al. 2002, AJ, 124, 2364
Kimball, A. E., & Ivezić, Ž. 2008, AJ, 136, 684
Komissarov, S. S., & Gubanov, A. G. 1994, A&A, 285, 27
Krueger, T. K., Aller, L. H., & Czyzak, S. J. 1970, ApJ, 160, 921
Krug, H. B., Rupke, D. S. N., & Veilleux, S. 2010, ApJ, 708, 1145
Lal, D. V., & Ho, L. C. 2010, AJ, 139, 1089
Leitherer, C., & Heckman, T. M. 1995, ApJS, 96, 9
Liu, X., Shen, Y., Strauss, M. A., & Greene, J. E. 2010, ApJ, 708, 427
Liu, X., Zakamska, N. L., Greene, J. E., Strauss, M. A., Krolik, J. H., & Heckman, T. M. 2009, ApJ, 702, 1098
Lonsdale, C. J., Lonsdale, C. J., Smith, H. E., & Diamond, P. J. 2003, ApJ, 592, 804
Magorrian, J., Tremaine, S., Richstone, D., Bender, R., Bower, G., Dressler, A., Faber, S. M., Gebhardt, K., Green, R., Grillmair, C., Kormendy, J., & Lauer, T. 1998, AJ, 115, 2285
Martin, C. L. 1998, ApJ, 506, 222
—. 2005, ApJ, 621, 227
Martini, P. 2004, in in Coevolution of Black Holes and Galaxies (Cambridge: Cambridge University Press), ed. L. C. Ho, 169
Martini, P., & Weinberg, D. H. 2001, ApJ, 547, 12
Matheson, T., et al. 2008, AJ, 135, 1598
McNamara, B. R., & Nulsen, P. E. J. 2007, ARA&A, 45, 117

Moe, M., Arav, N., Bautista, M. A., & Korista, K. T. 2009, ApJ, 706, 525
Morić, I., Smolčić, V., Kimball, A., Riechers, D. A., Ivezić, Ž., & Scoville, N. 2010, ApJ, 724, 779
Nesvadba, N. P. H., Lehnert, M. D., De Breuck, C., Gilbert, A. M., & van Breugel, W. 2008, A&A, 491, 407
Nesvadba, N. P. H., Lehnert, M. D., Eisenhauer, F., Gilbert, A., Tecza, M., & Abuter, R. 2006, ApJ, 650, 693
Osterbrock, D. E., & Ferland, G. J. 2006, Astrophysics of gaseous nebulae and active galactic nuclei
Proga, D., Stone, J. M., & Kallman, T. R. 2000, ApJ, 543, 686
Reyes, R., Zakamska, N. L., Strauss, M. A., Green, J., Krolik, J. H., Shen, Y., Richards, G. T., Anderson, S. F., & Schneider, D. P. 2008, AJ, 136, 2373
Richards, G. T., et al. 2006, ApJS, 166, 470
Rupke, D. S., Veilleux, S., & Sanders, D. B. 2005a, ApJ, 632, 751
—. 2005b, ApJS, 160, 115
Rupke, D. S. N., & Veilleux, S. 2011, ApJ, 729, L27
Sanders, D. B., & Mirabel, I. F. 1996, ARA&A, 34, 749
Sanders, D. B., Soifer, B. T., Elias, J. H., Madore, B. F., Matthews, K., Neugebauer, G., & Scoville, N. Z. 1988, ApJ, 325, 74
Schmidt, G. D., Elston, R., & Lupie, O. L. 1992a, AJ, 104, 1563
Schmidt, G. D., Stockman, H. S., & Smith, P. S. 1992b, ApJ, 398, L57
Shapley, A. E., Steidel, C. C., Pettini, M., & Adelberger, K. L. 2003, ApJ, 588, 65
Shen, Y., Liu, X., Greene, J. E., & Strauss, M. A. 2011, ApJ, 735, 48
Smith, P. S., Schmidt, G. D., Hines, D. C., & Foltz, C. B. 2003, ApJ, 593, 676
Springel, V., Di Matteo, T., & Hernquist, L. 2005, MNRAS, 361, 776
Stockton, A., & MacKenty, J. W. 1987, ApJ, 316, 584
Sturm, E., et al. 2011, ApJ, 733, L16
Tremonti, C. A., Moustakas, J., & Diamond-Stanic, A. M. 2007, ApJ, 663, L77
Tremonti, C. A., et al. 2004, ApJ, 613, 898
van Dokkum, P. G. 2001, PASP, 113, 1420
Veilleux, S., Cecil, G., & Bland-Hawthorn, J. 2005, ARA&A, 43, 769
Veilleux, S., Cecil, G., Bland-Hawthorn, J., Tully, R. B., Filippenko, A. V., & Sargent, W. L. W. 1994, ApJ, 433, 48
Villar-Martín, M., Tadhunter, C., Pérez, E., Humphrey, A., Martínez-Sansigre, A., Delgado, R. G., & Pérez-Torres, M. 2010, MNRAS, 407, L6
Wardle, J. F. C., & Kronberg, P. P. 1974, ApJ, 194, 249
Weiner, B. J., et al. 2009, ApJ, 692, 187
Xu, C., Livio, M., & Baum, S. 1999, AJ, 118, 1169
York, D. G., et al. 2000, AJ, 120, 1579
Zakamska, N. L., Gómez, L., Strauss, M. A., & Krolik, J. H. 2008, AJ, 136, 1607
Zakamska, N. L., Strauss, M. A., Heckman, T. M., Ivezić, Ž., & Krolik, J. H. 2004, AJ, 128, 1002
Zakamska, N. L., et al. 2003, AJ, 126, 2125
—. 2005, AJ, 129, 1212
—. 2006, AJ, 132, 1496